Liquid jet generation and break-up

C. Baranger
CMLA, CNRS UMR 8536
& ENS Cachan
61, av. du Pdt Wilson
94235 Cachan CEDEX

G. Baudin
Centre d'Études de Gramat
DGA
46500 Gramat

L. Boudin, B. Després, F. Lagoutière
Laboratoire J.-L. Lions
CNRS UMR 7598 & Univ. Paris-VI
Boîte courrier 187
75252 Paris CEDEX 05

E. Lapébie
Centre d'Études de Gramat
DGA
46500 Gramat

T. Takahashi
Institut Élie Cartan
Univ. Nancy-I
B.P. 239
54506 Vandœuvre-lès-Nancy CEDEX

Abstract. This work is motivated by the numerical simulation of the generation and break-up of droplets after the impact of a rigid body on a tank filled with a compressible fluid. This paper splits into two very different parts. The first part deals with the modeling and the numerical resolution of a spray of liquid droplets in a compressible medium like air. Phenomena taken into account are the breakup effects due to the velocity and pressure waves in the compressible ambient fluid. The second part is concerned with the transport of a rigid body in a compressible liquid, involving reciprocal effects between the two components. A new one-dimensional algorithm working on a fixed Eulerian mesh is proposed.

The GENJET (GENeration and breakup of liquid JETs) project has been proposed by the Centre d'Études de Gramat (CEG) of the Délégation Générale de l'Armement (DGA). It concerns the general study of the consequences of a violent impact of a rigid body against a reservoir of fluid. Experiments show that once the solid has pierced the shell of the reservoir, it provokes a dramatic increase of the pressure inside the reservoir, whose effect is the ejection of some fluid through the pierced hole. The generated liquid jet then expands into the ambient air, where it can interact with some air pressure waves, leading to a fragmentation of the jet into small droplets. These experiments show that after having pierced the shell, the projectile behaves as a rigid body. They also show that the liquid inside the reservoir behaves as a compressible fluid (indeed, the projectile velocity, around 1000 $m.s^{-1}$, is in the same order of magnitude than the sound speed in the liquid).

The modeling of such a complex flow requires to take into account very different regimes, from the pure compressible and/or incompressible flow condition to a droplet regime (such a regime sharing some similarities with kinetic modeling of

particles). Moreover many scales are needed to correctly describe the complete experiments, from the large hydrodynamic scale to the small droplet scale. The study done during CEMRACS 2004 focused on the fluid regime and on the droplet regime, since some important difficulties are still there for both regimes separately.

- Concerning the breakup of droplets in the air, we have focused on physical and numerical modeling issues.
- Concerning the fluid regime, an important difficulty at the numerical level is that we want to get an accurate numerical description of the transport of a rigid body inside a compressible fluid. Even if the rigid body is of course not a fluid, the situation shares at the numerical level a lot of similarities with the coupling an incompressible fluid with a compressible one. Thus this part of the study concerns more numerical algorithms than the modeling.

The present paper follows this cutout of the study. Section 1 presents the modeling of the breakup of droplets, whereas section 2 treats the coupling of the rigid body and the fluid. In both sections, numerical results are reported.

In view of the main goal of the GENJET project, a natural perspective of the work described below would be the coupling of the models, algorithms and numerical methods.

1. A kinetic modeling of a breaking up spray with high Weber numbers

In this section, we aim to model a spray of droplets which evolve in an ambient fluid (typically the air). That kind of problem was first studied by Williams for combustion issues [32]. The works of O'Rourke [20] helped to set the modeling of such situations and their numerical simulation through an industrial code, KIVA [1].

The main phenomenon that occuring in the spray is the breakup of the droplets. Any other phenomena, such as collisions or coalescence, will be neglected in this work, but they are reviewed in [3] for example. Instead of using the TAB model (see [2]), which is more accurate for droplets with low Weber numbers, we choose the so-called Reitz wave model [27], [21], [4]. Then this breakup model is taken into account in a kinetic model [14], [2].

The question of the spray behavior with respect to the breaking up has arised in the context of the French military industry. One aims to model with an accurate precision the evolution of a spray of liquid droplets inside the air. In that situation, the droplets of the spray are assumed to remain incompressible (the mass density ρ_d is a constant of the problem) and spherical. We also assume that the forces on the spray are negligible with respect to the drag force, at least at the beginning of the computations. After a few seconds, the gravitation may become preponderant. Note that the aspects of energy transfer will not be tackled in this report.

$t \geq 0$	time
$x \in \mathbb{R}^{d_x}$	position
$v \in \mathbb{R}^{d_v}$	droplet velocity
$r \in]0, +\infty[$	droplet radius
σ	surface tension of the droplet
$f(t, x, v)$	spray probability density function (PDF)
Q_{bup}	breakup operator
ρ_d	droplet mass density (constant)
$m = \frac{4}{3}\pi r^3 \rho_d$	droplet mass
$\rho_g(t, x)$	fluid density
$u(t, x) \in \mathbb{R}^{d_v}$	fluid flow velocity
$\alpha(t, x)$	fluid volume fraction
C_d	drag coefficient
Re	Reynolds number associated to the fluid near a droplet
Re_d	Reynolds number of a droplet
We	Weber number associated to the gas near a droplet
We_d	Weber number of a droplet
Oh	Ohnesorge number
Ta	Taylor number

Table 1: Notations

In the subsection 1.1, we derive the equations of the model and check the properties of conservation of mass and momentum. Then we briefly present the scheme for the numerical resolution of our problem. Eventually, we show some numerical results.

The notations used in the first section are presented in table 1.

1.1. Presentation of the model

The spray is described by the probability density function (PDF) f, which depends on time t, position x, velocity v and radius r. The number of droplets located in the volume (of the phase space) $[x, x + dx] \times [v, v + dv] \times [r, r + dr]$ is the quantity $f(t, x, v, r)dxdvdr$.

The PDF f satisfies the kinetic equation

$$\partial_t f + v \cdot \nabla_x f + \nabla_v \cdot (f\gamma) + \partial_r (f\chi) = Q_{\text{bup}}(f). \tag{1.1}$$

The acceleration γ of one droplet is given by

$$\gamma(t, x, v, r) = -\frac{1}{m(r)} D(t, x, v, r)(v - u(t, x)), \tag{1.2}$$

where m is the droplet mass, u the fluid velocity and

$$D = \frac{\pi}{2} r^2 \rho_g C_d |v - u|.$$

The coefficient C_d is the drag coefficient, and its value is given in the appendix.

In order to give an explicit form of χ and Q_{bup}, we here need to explain how the breakups are handled by the Reitz wave model. We here use the classical Reynolds (Re, Re_d), Weber (We, We_d), Ohnesorge (Oh) and Taylor (Ta) numbers, whose values are described below (see [26], for instance). One can use two different Reynolds numbers: the Reynolds number associated to the fluid near a droplet, and the Reynolds number of the droplet itself. We have

$$\text{Re} = \frac{r\rho_g |v - u|}{\mu_g}, \qquad \text{Re}_d = \frac{r\rho_d |v - u|}{\mu_d},$$

where μ_g (resp. μ_d) is the fluid (resp. droplet) viscosity. In the same way, we consider two different Weber numbers

$$\text{We} = \frac{r\rho_g |v - u|^2}{\sigma_d}, \qquad \text{We}_d = \frac{r\rho_d |v - u|^2}{\sigma_d},$$

where σ_d is the surface tension of the droplet. Then it is easy to define the Ohnesorge and Taylor numbers of the droplet

$$\text{Oh} = \frac{\sqrt{\text{We}_d}}{\text{Re}_d}, \qquad \text{Ta} = \text{Oh}\sqrt{\text{We}}.$$

We refer to [5] for instance, for the definition of the drag coefficient C_d.

A breaking up droplet looses some mass by creating small children droplets, but does not disappear, as it occurs in most breakup models. Hence, there is no disappearance of droplets, only production, since only the mother droplet's radius changes: we must be able to compute the new radius of the mother droplet (thanks to χ) and to evaluate the characteristics of the children droplets (number, position, velocity, radii). The phenomenon taken into account is the main disturbance on the surface of the droplet, which is most likely to result in breakup. The wavelength of this disturbance is

$$\Lambda = \frac{9.02\left(1 + 0.45\sqrt{\text{Oh}}\right)\left(1 + 0.4\text{Ta}^{0.4}\right)}{\left(1 + 0.865\text{We}^{5/3}\right)^{0.6}}\, r. \tag{1.3}$$

We also need the growth rate of the wavelength

$$\Omega = \frac{0.34 + 0.385\text{We}^{3/2}}{(1 + \text{Oh})\left(1 + 1.4\text{Ta}^{0.6}\right)}\sqrt{\frac{\sigma}{\rho_d r}}, \tag{1.4}$$

where σ is the surface tension of the droplet.

We can then provide a characteristic breakup time

$$\tau = \frac{C_\tau r}{\Omega\Lambda}, \tag{1.5}$$

where C_τ mainly depends on the characteristic lengths of the spray. We here propose to choose $C_\tau = 37.88$. Note that (1.3)–(1.5) come from [4], as well as this value of C_τ. This choice seems to be significant, since the physical setting of [4] is close to ours.

Eventually, the variation χ of the droplet radius satisfies

$$\chi(t,x,v,r) = -\nu(t,x,v,r)(r - R(t,x,v,r)), \tag{1.6}$$

where $R = C_R\Lambda$ (we here choose $C_R = 0.61$). The breakup frequency ν is given by

$$\begin{array}{rcll} \nu & = & 0 & \text{if } r \leq \Lambda \text{ or } \mathrm{We} \leq \dfrac{1}{2}\sqrt{\mathrm{Re}}, \\ \nu & = & \dfrac{1}{\tau} & \text{in any other cases.} \end{array} \tag{1.7}$$

Note that (1.6) cannot be seen as a linear ODE on r: even if R linearly depends on Λ, the wavelength itself does not linearly depend on r, since in (1.3), the Ohnesorge, Taylor and Weber numbers also depend on r.

The breakup operator only deals with the small children droplets. We then propose the following definition of Q_{bup}, where we only keep the dependencies on the velocity and the radius, for the sake of simplicity,

$$\begin{array}{rcl} Q_{\mathrm{bup}}(f)(v,r) & = & \displaystyle\int_{v_*,r_*} \int_{\mathcal{S}_1(v_*)} \nu(v_*,r_*) \frac{3{r_*}^2(r_* - R_*)}{{R_*}^3} \\ & & \qquad \delta_{V_*}(v)\ \delta_{R_*}(r)\ f(v_*,r_*)\ \dfrac{ds}{2\pi}\ dr_* dv_*, \end{array} \tag{1.8}$$

where $V_* = v_* + v_\perp n$, with $v_\perp = C_V\Lambda\Omega$ ($C_v = 0.5$, in our problem) and n is a random vector of the unit disc $S_1(v_*)$ of the linear plane normal to the vector v_*.

1.2. Conservations

In this subsection, we check that the classical properties of conservations of mass and momentum are satisfied.

Proposition 1.1. The total mass of the spray is constant (in time).

Proof. Let us denote by $M(t)$ the total mass of the spray at time t. We immediately have

$$\begin{array}{rcl} \dfrac{dM}{dt} & = & \dfrac{4\pi\rho_d}{3} \displaystyle\int_{x,v,r} \partial_t f \cdot r^3\ drdvdx \\ & = & \dfrac{4\pi\rho_d}{3} \left[-\displaystyle\int_{x,v,r} \partial_r(f\chi) r^3\ drdvdx + \int_{x,v,r} Q_{\mathrm{bup}}(f) r^3\ drdvdx \right], \end{array}$$

with the disappearance of the conservative terms on x and v. Then, by a standard computation, and using (1.6) and (1.8), we get

$$\begin{aligned}\frac{dM}{dt} &= 4\pi\rho_d\Bigg[-\int_{x,v,r} f(v,r)\nu(v,r)(r-R)\ r^2\ drdvdx \\ &\quad+\int_{x,v,r}\left(\int_{v_*,r_*}\int_{\mathcal{S}_1(v_*)}\nu(v_*,r_*)\frac{{r_*}^2(r_*-R_*)}{{R_*}^3}\ r^3\delta_{V_*}(v)\ \delta_{R_*}(r)\right. \\ &\qquad\left.f(v_*,r_*)\ \frac{ds}{2\pi}\ dr_*dv_*\right)\ drdvdx\Bigg].\end{aligned}$$

The integration along $S_1(v_*)$ gives 1, and the one on v against the Dirac mass too. It is then clear that

$$\begin{aligned}\frac{dM}{dt} &= 4\pi\rho_d\Bigg[-\int_{x,v,r} f(v,r)\nu(v,r)(r-R)\ r^2\ drdvdx \\ &\quad+\int_{x,v_*,r_*}\nu(v_*,r_*)\frac{{r_*}^2(r_*-R_*)}{{R_*}^3}\ {R_*}^3 f(v_*,r_*)\ dr_*dv_*dx\Bigg],\end{aligned}$$

that ends the proof.

Since the fluid acts on the spray, the total momentum of the spray is not constant, but we have the following

Proposition 1.2. The time derivative of the total momentum of the spray equals the mean force of the fluid on the spray.

Proof. Let us denote by $I(t)$ the total momentum of the spray at time t. We immediately have

$$\begin{aligned}\frac{dI}{dt} &= \frac{4}{3}\pi\rho_d\int_{x,v,r} f\gamma r^3 drdvdx \\ &\quad+4\pi\rho_d\Bigg[-\int_{x,v,r} f(v,r)\nu(v,r)(r-R)\ r^2 v\ drdvdx \\ &\qquad+\int_{x,v,r}\left(\int_{v_*,r_*}\int_{\mathcal{S}_1(v_*)}\nu(v_*,r_*)\frac{{r_*}^2(r_*-R_*)}{{R_*}^3}\ r^3 v\ \delta_{V_*}(v)\ \delta_{R_*}(r)\right. \\ &\qquad\left.f(v_*,r_*)\ \frac{ds}{2\pi}\ dr_*dv_*\right)\ drdvdx\Bigg].\end{aligned}$$

The first integral term is exactly the mean force of the fluid on the spray. Let us denote by J the term inside the brackets and show that it equals 0. By similar computations, we obtain that

$$\begin{aligned}J &= -4\pi\rho_d\int_{x,v,r} f(v,r)\nu(v,r)(r-R)\ r^2 v\ drdvdx \\ &\quad+4\pi\rho_d\int_{x,v_*,r_*}\int_{\mathcal{S}_1(v_*)}\nu(v_*,r_*)f(v_*,r_*){r_*}^2(v_*+v_\perp n)\ \frac{ds}{2\pi}\ dr_*dv_*dx.\end{aligned}$$

Since

$$\int_{\mathcal{S}_1(v_*)} n \, \frac{ds}{2\pi} = 0,$$

it becomes clear that $J = 0$ and the proof is ended.

The well-posedness of (1.1) is not investigated in this paper. However, such a question is studied for other breakup operators, as in [14].

1.3. Numerical tests

We do not here take into account the motion of the droplets. Nevertheless, we aim to ensure the compatibility of the particle method used here, with any finite volume method fitted to the surrounding fluid.

1.3.1. Numerical scheme We first start by a description of the numerical scheme used for solving (1.1). We assume that the particles have three-dimensional velocities.

The numerical scheme is time-split into two steps: the transport (in velocity) and the breakup. That means that we successively solve

$$\partial_t f + \partial_r(f\chi) = Q_{\text{bup}}(f), \tag{1.9}$$

and

$$\partial_t f + \nabla_v \cdot (f\gamma) = 0, \tag{1.10}$$

during a whole time step. Since we use a particle method, the PDF f is sought to be under the form

$$f(t, v, r) = \omega \sum_{p=1}^{P(t)} \delta_{v_p(t)}(v)\, \delta_{r_p(t)}(r),$$

where $(v_p(t), r_p(t))$ respectively denote the velocity and the radius of a numerical particle p at a time t, $P(t)$ is the total number of numerical particles and ω is the representativity of the particles (constant in this work).

Transport. During the first part of a time step, we follow the movement of the particles along their characteristics (in terms of velocity, not radius), i.e. we solve

$$\frac{dv_p}{dt} = -\frac{1}{m_p} D_p(v_p - u).$$

Then, the time discretization gives:

$$v_p^{n+1} = v_p^n - \frac{\Delta t}{m_p} D_p^n (v_p^{n+1} - u^n),$$

where u^n is the velocity of the fluid at time $n\Delta t$. We here use an implicit scheme for the discretization of $\frac{dv_p}{dt}$, in order to ensure the numerical stability.

Breakup. The second part of the splitting is the breakup step. This is a linear process, that is, for each particle p, it happens as follows.

1. If $r_p^n \leq C_R \Lambda_p^n$ then the particle p remains as it is.

2. If $r_p^n > C_R \Lambda_p^n$ and $\mathrm{We}_p^n \leq \frac{\sqrt{\mathrm{Re}_i^n}}{2}$ then the particle p remains as it is.

3. In the other cases, a breakup occurs with the probability $\Delta t / \nu_p^n$. If a breakup occurs,

   (a) the radius of the particle evolves: $r_p^{n+1} = \frac{\tau_p^n r_p^n + \Delta t C_R \Lambda_p^n}{\tau_p^n}$

   (b) the total number of the new particles created by the breakup of a particle p is computed in order to ensure the mass conservation $N_p = \frac{3 {r_p^n}^2 (r_p^n - R_p^n)}{{R_p^n}^3}$, and with the radius $R_p^n = C_R \Lambda_p^n$,

   (c) N_p particles $\tilde{p}$ are created with position $x_{\tilde{p}}^{n+1} = x_p^n$, radius $r_{\tilde{p}}^{n+1} = R_p^n$ and velocity $v_{\tilde{p}}^{n+1} = v_p^n + C_V \Lambda_p^n \Omega_p^n \vec{n}$ ($\vec{n}$ unit vector normal to v_p^n).

1.3.2. Numerical simulations The simulations that we made do not take into account the simulation of the surrounding fluid. First, we only compute the breakup of some droplets which remain motionless. Second, we compute the breakup and the transport of the droplets.

Breakup. We here aim to study the influence of the velocity of the surrounding fluid on the breakup phenomenon (number of breakups, number and size of the created droplets). We have several possibilities for the value of the velocity of the fluid: either it is a constant (equal to 0) during the whole computation, or there could be a shock (in our example, $|u|$ increases from 0 to $400\,\mathrm{m.s}^{-1}$ at a given time), or it could follow a linear profile in time. These three cases are described below.

1. In the first simulation, the fluid is motionless ($u \equiv 0$). Initially, the radii of the 100 droplets considered are uniformly distributed between 0.5 and 1 mm and the velocities are equal to $50\,\mathrm{m.s}^{-1}$ in one direction. The computation lasts for 0.1 s, but actually there is no fragmentation after 0.06 s. The 100 particles become 8000 with a radius around 0.17 mm (between 0.1725 and 0.1775 mm, the higher radii correspond to the "mother" droplets). We could see in figure 1 the initial and final distributions of the radii.

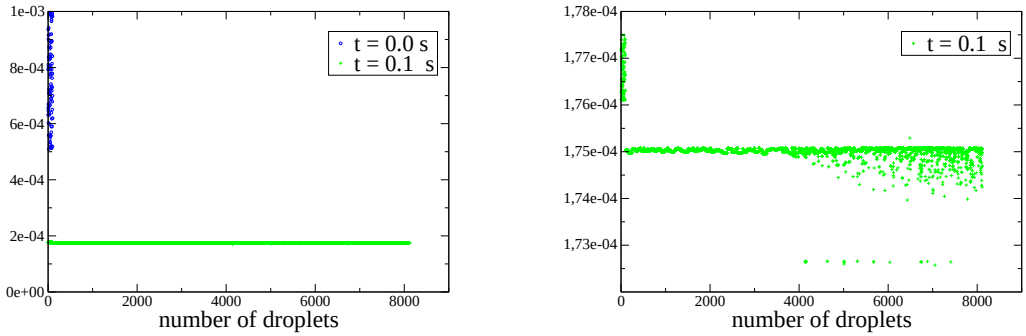

Figure 1: Radii (m) of the particles with a fixed surrounding fluid.

2. The second simulation consists in including a shock in the fluid: the velocity of the fluid decreased from 0 to $-400\,\mathrm{m.s^{-1}}$ at time 0.04 s. For the sake of the computation, the initial distribution of the radii of the 100 droplets is chosen to be smaller because of the high number of created droplets at this relative velocity (around $350\,\mathrm{m.s^{-1}}$). So we start with radii around 5 and $10\,\mu$m. At the end, the radii of the droplets is between 2.54 and $2.62\,\mu$m.

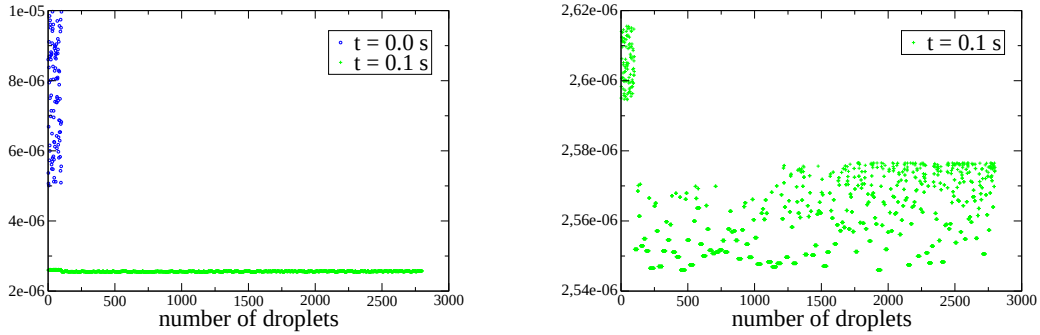

Figure 2: Radii (m) of the particles with a shock in the fluid.

3. In the last simulation, the velocity of the surrounding fluid linearly decreases from 0 to $-400\,\mathrm{m.s^{-1}}$ and from $t = 0.04$ to 0.05 s. We here keep the same

initial radius distribution than in the previous simulation. There are less particles created. In figure 3, we note that several values of radii are pointed out ($2.4\,\mu$m, $2.6\,\mu$m and $2.8\,\mu$m approximately). As a matter of fact, the continuous linear profile of the fluid velocity is discretized into piecewise constant values with respect to the time steps. To avoid this numerical artefact, one must refine the time steps.

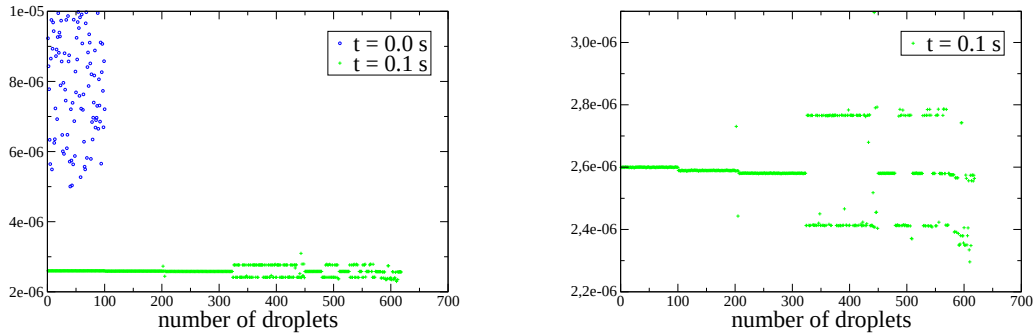

Figure 3: Radii (m) of the particles with a linearly profiled velocity for the fluid.

To conclude this part, we could say that there is a mean radius for the created droplets which depends on the relative velocity between the droplets and the fluid (for example, around 10^{-4} m without shock, and 10^{-6} m when a shock occurs in the fluid). The radii seems to correspond to the physical behavior of a spray when a shock occurs in the air, i.e. the 'atomization' of the spray, detected during some experimentations made at the CEG.

Breakup and transport. We made some computations of the phenomena: breakup and transport of the droplets. For the time step (verifying a CFL condition) in the transport step, we assume that the size of a cell is around 0.005 mm (200 cells for 1 meter). In order to take the interaction between these phenomena into account (because the breakup time is larger than the transport time), the initial radii are randomly picked between 10 and 20 mm. Of course there is some breakup in the beginning, but as the velocity of the droplets goes to 0 (the velocity of the surrounding fluid), there are less and less breakups. On figure 4, we could see the final distribution of the droplets, and on figure 5, the successive positions of the droplets at several times.

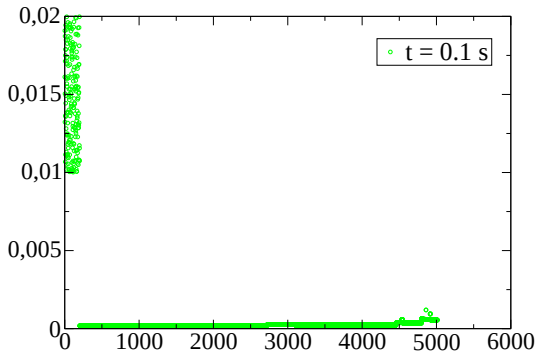

Figure 4: Final radii of the droplets during the transport-breakup computation.

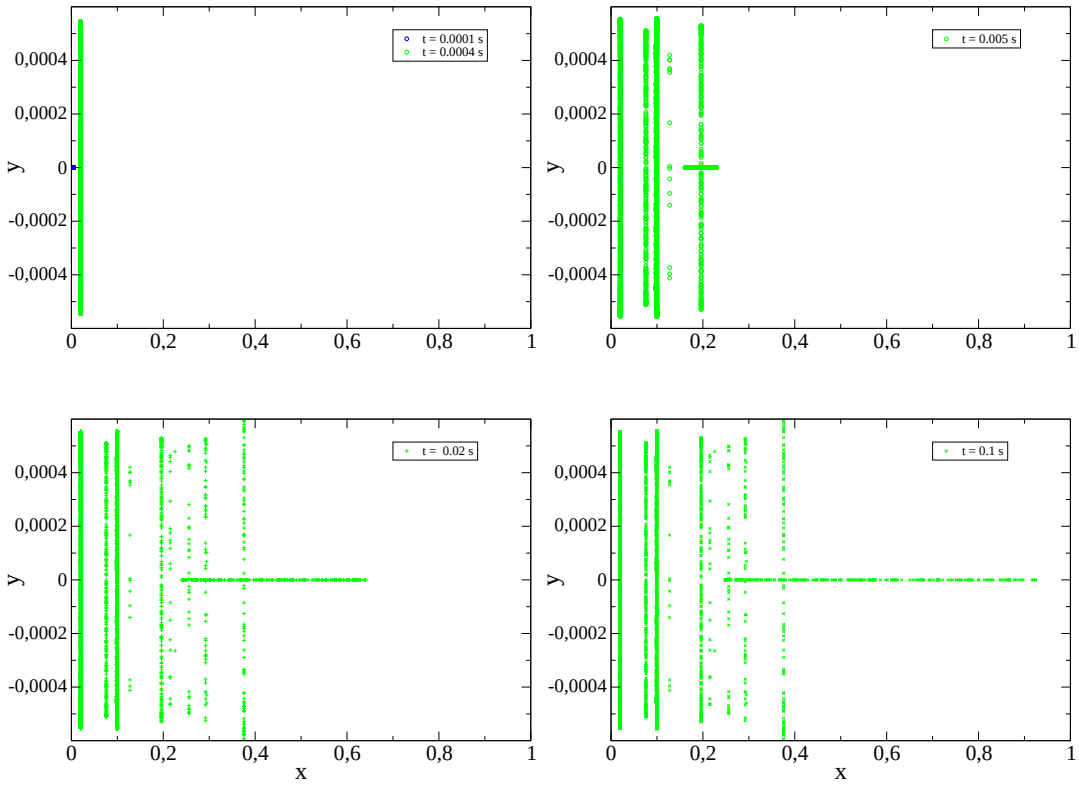

Figure 5: Positions of the droplets during the transport-breakup computation.

2. Fluid-structure coupling

The general context of this section is the transport of a rigid body in a compressible fluid, including the coupling effects.

The compressible fluid under consideration is governed by the Euler system of partial differential equations, with ideal or stiffened gas pressure law. The goal is to take into account the coupling effects between the solid and the fluid.

Let us briefly present some of the most used methods for the numerical resolution of fluid-structure coupling.

- One of the most known methods, the Immersed Boundary Method, was initiated by Peskin in [22] for blood flow in heart computations and then have had a lot of improvements for other applications: see [23] for a survey, [19] for another recent development. These applications concern coupling between an elastic or rigid solid and an *incompressible* fluid where, for the numerical stability, the velocity is assumed to be regular enough (otherwise a CFL-like condition would be very restrictive: see the discussion on the hyperbolicity and on the numerical stability in the following). This method thus cannot be envisaged for the present problem.

- Among other existing methods, let us mention the Fat Boundary Method of Maury, Maury and Ismail: [18] (for the Poisson problem) and [15] (for incompressible fluid problems), also dedicated to incompressible fluids. A fictitious domain method is used in [11]. Another method, proposed in [28], uses a fixed mesh like the fictitious domain, and considers a global mixed formulation (for the fluid and the solid) where the condition of rigidity of the solid is imposed on the finite element spaces. The major drawback of these last three methods for handling *compressible* fluids is their lack of conservativity.

- The method of Piperno, Farhat, etc. (see for example [9], [24], [25]) is conservative in mass and momentum. The coupling algorithm there described uses an Arbitrary Lagrangian Eulerian (ALE) formalism with a moving mesh (typically a mesh following the solid). A precise analysis of this type of methods has been done by Piperno. Nevertheless, the aim of the present CEMRACS project is to do computations on a motionless Cartesian mesh which is the same for the solid and the fluid. We thus abandon these methods (note that another ALE method is used in [17] for particle transport in an incompressible medium).

- A penalisation procedure coupled with a Volume Of Fluid (VOF) algorithm for the transport of the volume fraction has been developed in [31]. It has the little drawback of allowing artificial deformation of the solid in spite of the penalisation and of the non dissipative VOF method. Furthermore, it seems that the method has not been used for compressible fluids yet. From another point of view, it has been shown in previous numerical experiments

that replacing the undeformable solid with a fluid or a *very* rigid body and to use a bi-fluid or a fluid-elastodynamic code (which is similar to a penalisation procedure) was not a good solution when computing strong shocks (this leads to an over-evaluation of the deceleration of the body in the fluid). Thus we decide to really consider the solid as undeformable, both in the mathematical equations and in the final code.

The method we developed is based on an explicit finite volume scheme on a Eulerian unique mesh. The presence of mixed cells (containing solid *and* fluid: this is due to the projection of the moving solid on the fixed mesh) leads to use a mixture model that takes into account the undeformable behavior of the solid.

This part of the paper is organized as follows: subsection 2.1 gives the mathematical model governing the fluid-solid system, taking into account the compressible behavior of the fluid (ideal or stiffened gas), the undeformability of the solid, and the coupling effects; subsection 2.2 presents a mathematical way to take into account the presence of mixed cells that necessarily appear in the numerical stage (on a fixed grid); we then propose a rapid mathematical analysis of this model, in subsection 2.3; the numerical scheme is developed in subsection 2.4; subsection 2.5 shows some numerical results in dimension one.

2.1. The system fluid-rigid body

Let us denote by $\Omega \subset \mathbb{R}^3$ the domain of interest. The solid body is assumed to be a connex region $S(t) \subset \mathbb{R}^3$ (for any time $t \in [0,T]$) such that $S(t) \cap \partial\Omega = \emptyset$. Thus, the fluid occupies the region $\Omega \setminus S(t)$. The medium in $\Omega \setminus S(t)$ is supposed to be governed by the compressible Euler equations (conservations of mass, momentum and total energy), the region $S(t)$ evolves following a rigid solid displacement law: it can be decomposed into a translation and a rotation. These two parameters are computed with the help of the action of the fluid on the solid. The action of the solid onto the the fluid is taken into account by considering some "wall-condition" on $\partial\Omega$: friction between the fluid and the solid are neglected (so as the friction inside the fluid). For the Eulerian fluid, we use the variables ρ_1, u_1 and e_1 for respectively, the density, the velocity and the total energy. The density of the solid is constant in time and space. For the solid, we use the variables h, ω for respectively the center of mass and the angular velocity. If we denote by $Q(t)$ the matrix of rotation of the rigid body, i.e.

$$\dot{Q}(t)x = \omega(t) \wedge (Q(t)x)\,, \quad \forall x \in \mathbb{R}^3,$$

then, we can describe the domain $S(t)$ of the solid at time t by using the domain S occupied by the solid at the initial time:

$$S(t) = \{Q(t)y + h(t), \quad y \in S\}\,.$$

In the sequel, we denote by $n(x,t)$ the unit normal vector to $\partial S(t)$ at the point x directed to the interior of the rigid body. We also introduce the mass M of the

solid and J its inertial matrix. The equations of the solid are obtained by applying the conservation of linear and angular momentum (Newton's laws).

With the above notations, the equations modeling the movement of the fluid and of the rigid body can be written in the following form:

$$\begin{cases} \partial_t \rho_1 + \operatorname{div}(\rho_1 u_1) = 0, & \text{in } \Omega \setminus S(t), \\ \partial_t(\rho_1 u_1) + \operatorname{div}(\rho_1 u_1^2 + p_1) = 0, & \text{in } \Omega \setminus S(t), \\ \partial_t(\rho_1 e_1) + \operatorname{div}(\rho_1 u_1 e_1 + p_1 u_1) = 0, & \text{in } \Omega \setminus S(t), \\ u_1 \cdot n = h' \cdot n, & \text{on } \partial S(t), \\ Mh''(t) = \displaystyle\int_{\partial S(t)} p_1 n \, \mathrm{d}\sigma_x, & \\ (J\omega)'(t) = \displaystyle\int_{\partial S(t)} (x - h(t)) \wedge p_1 n \, \mathrm{d}\sigma_x & \end{cases} \tag{2.11}$$

where $\mathrm{d}\sigma_x$ is the induced measure on $\partial S(t)$. The first 3 equations are the classical Euler system for a compressible fluid. The fourth one ensures the continuity of the normal velocity on the solid boundary; and the last two ones describe the Newton laws for the solid. In this system, p_1 is the pressure inside the fluid and is given by the model of the fluid. Here, we consider the case of a stiffened gas, whose law is given by $p_1 = (\gamma_1 - 1)\rho_1 \left(e_1 - \frac{u_1^2}{2}\right) - \gamma_1 \pi_1$, with $\gamma_1 > 1$, $\pi_1 \geq 0$ (the case $\pi_1 = 0$ corresponding to an ideal gas). Let us now introduce classical notations: $\varepsilon_1 = e_1 - u_1^2/2$, the internal energy, and $\tau_1 = 1/\rho_1$, the specific volume.

We now simplify this system, assuming slab symmetry (as will be done in the numerical subsections). We suppose that the domain of the whole system is $[0, 1]$ and we denote by $B(t) = [a(t), b(t)]$ the domain of the rigid body. We always assume that $0 < a(t) < b(t) < 1$ (with $b(t) - a(t) = b(0) - a(0)$). Therefore, the domain of the fluid is

$$\Omega(t) = [0, 1] \setminus [a(t), b(t)].$$

The density of the solid is constant and thus the position of the center of mass of the rigid body is $h(t) = \dfrac{a(t) + b(t)}{2}$. We also denote by M the mass of the solid.

In Eulerian coordinates, the equations modeling the movement of the system can be written as follows:

$$\partial_t(\rho_1) + \partial_x(\rho_1 u_1) = 0 \qquad x \in \Omega(t),\ t \in [0, T], \tag{2.12}$$

$$\partial_t(\rho_1 u_1) + \partial_x(\rho_1 u_1^2 + p_1) = 0 \qquad x \in \Omega(t),\ t \in [0, T], \tag{2.13}$$

$$\partial_t(\rho_1 e_1) + \partial_x(\rho_1 u_1 e_1 + p_1 u_1) = 0 \qquad x \in \Omega(t),\ t \in [0, T], \tag{2.14}$$

$$u_1(t) = h'(t) \qquad x \in \{a(t), b(t)\},\ t \in [0, T], \tag{2.15}$$

$$Mh''(t) = p_1(b(t)) - p_1(a(t)) \qquad t \in [0, T], \tag{2.16}$$

$$\rho_1(x, 0) = \rho_1^0(x), \qquad x \in \Omega(0), \tag{2.17}$$

$$u_1(x, 0) = u_1^0(x), \qquad x \in \Omega(0), \tag{2.18}$$

$$e_1(x, 0) = e_1^0(x), \qquad x \in \Omega(0), \tag{2.19}$$

$$h(0) = h^0 \in \mathbb{R},\ h'(0) = h^1 \in \mathbb{R}. \tag{2.20}$$

2.2. An approximate system involving mixing

The numerical strategy that will be chosen in subsection 2.4 involves a fixed grid. For this reason, the solid and the fluid may occupy only parts of cells: the mass fractions of solid and fluid become real numbers in $[0, 1]$ once it is projected on the grid. This subsection is devoted to the writing of a mathematical model allowing this artificial mixing. We here introduce the mass fractions c_1 of the fluid and c_2 of the solid. These quantities are such that $c_1 + c_2 = 1$.

For the sake of simplicity, we limit the presentation to the dimension 1 and do not insist on the treatment of the solid region (where $c_1 = 1$, $c_2 = 0$).

The conservation equations are these of each component mass, global momentum and global energy. Let us denote as ρ the global density. The partial densities of each component are then $c_1\rho$ and $c_2\rho$. The mixing between the two components being only a numerical artefact, it is possible to determine the specific volume of the components, $\tau_1 = 1/\rho_1$ and $\tau_2 = 1/\rho_2$, and the additivity of volume leads to the equation $c_1\tau_1 + c_2\tau_2 = \tau = 1/\rho$ (cf. [16]). The system then reads

$$\begin{cases} \partial_t(c_1\rho) + \partial_x(c_1\rho u) = 0, \\ \partial_t\rho + \partial_x\rho u = 0, \\ \partial_t(\rho u) + \partial_x(\rho u^2 + p) = 0, \\ \partial_t(\rho e) + \partial_x(\rho u e + pu) = 0, \\ c_1 + c_2 = 1, \\ c_1\tau_1 + c_2\tau_2 = \tau. \end{cases} \tag{2.21}$$

where the unknows are c_1, c_2, ρ, u and e. We propose to compute the pressure p with $p = p_1(\tau_1, \varepsilon_1)$, which means that the solid has no influence on the fluid pressure. Recall that τ_2 is a constant and that ε_1 is computed with the help of $e = u^2/2 + \varepsilon_1$. System (2.21) is thus formally closed.

2.3. Mathematical study

The mathematical study of this system is very difficult and as far as we know, there is no result available in the literature. For the system fluid-rigid body with a viscous incompressible fluid modelled by the Navier-Stokes equations, several papers concerning the existence have been published in the last years (see, for example, [12], [13], [6], [29] and the references in [30]). In the case of a viscous compressible fluid, some results of existence can be found in [6] and [10].

This subsection is devoted to the computation of eigenvalues and eigenvectors of system (2.21) and to the analysis of its hyperbolicity. In order to simplify the analysis, we propose to use the Lagrangian formulation of (2.21). This formulation will be used for the derivation of the numerical scheme in subsection 2.4. It relies on the definition of the convective derivative $\mathrm{D}_t = \partial_t + u\partial_x$. In the regular case,

standard computations lead to the equivalent system

$$\begin{cases} \rho \mathrm{D}_t c_1 = 0, \\ \rho \mathrm{D}_t \tau = \partial_x u, \\ \rho \mathrm{D}_t u = -\partial_x p, \\ \rho \mathrm{D}_t e = -\partial_x (pu), \end{cases} \tag{2.22}$$

where τ_2 is a positive constant. This PDE system is closed via the algebraic relations $c_1 + c_2 = 1$, $c_1\tau_1 + c_2\tau_2 = \tau = 1/\rho$. Assuming the fluid has a strictly concave entropy $S_1(\tau_1, \varepsilon_1)$ verifying $\rho \mathrm{D}_t S_1 = 1/T \mathrm{D}_t \varepsilon_1 + p/T \mathrm{D}_t \tau_1 = 0$ where T is the temperature (which is the case for a stiffened gas, see below), we can symmetrize (2.22) with respect to pressure, writing

$$\mathrm{D}_t p_1 = \frac{\partial p_1}{\partial \tau_1} \mathrm{D}_t \tau_1 + \frac{\partial p_1}{\partial S_1} \mathrm{D}_t S_1 = \frac{\partial p_1}{\partial \tau_1} \mathrm{D}_t \tau_1$$

where p_1 is viewed as a function of τ_1 and S_1. Now recalling that $c_1\tau_1 + c_2\tau_2 = \tau$ and that τ_2 is constant, we get $\mathrm{D}_t \tau = c_1 \mathrm{D}_t \tau_1$, and, finally, $\rho \mathrm{D}_t p_1 = \omega \partial_x u$, where $\omega = 1/c_1 \partial p_1 / \partial \tau_1 < 0$ is defined if $c_1 > 0$. In Lagrangian coordinates, putting $\partial_m = \tau \partial_x$, the symmetrized system writes

$$\begin{cases} \mathrm{D}_t c_1 = 0, \\ \mathrm{D}_t p = \omega \partial_m u, \\ \mathrm{D}_t u = -\partial_m p, \\ \mathrm{D}_t S_1 = 0, \end{cases}$$

where the equation on the total energy has been replaced by the one on the entropy, and is completed with the algebraic equations $c_1 + c_2 = 1$, $c_1\tau_1 + c_2\tau_2 = 1/\rho$, $p = p_1 = (\gamma_1 - 1)\rho_1\varepsilon_1 - \gamma_1\pi_1$, $\varepsilon_1 = e - \frac{u^2}{2}$. This quasi-linear system writes $\mathrm{D}_t U = A \partial_m U$ with

$$U = \begin{pmatrix} c_1 \\ p \\ u \\ S_1 \end{pmatrix}, \quad A = \begin{pmatrix} 0 & 0 & 0 & 0 \\ 0 & 0 & \omega & 0 \\ 0 & -1 & 0 & 0 \\ 0 & 0 & 0 & 0 \end{pmatrix}.$$

The eigenvalues of A are 0, $\sqrt{-\omega}$ and $-\sqrt{-\omega}$, with eigenvectors $(1,0,0,0)^T$, $(0,0,0,1)^T$, $(0,-\sqrt{-\omega},1,0)^T$ and $(0,\sqrt{-\omega},1,0)^T$, which form a basis of $\mathbb{R}^4$, assuming $\omega \neq 0$, which is the case under the assumption $c_1 \in]0,1]$ and S_1 strictly concave. Hence we have the following

Proposition 2.1. *Assuming the existence of a strictly concave entropy, system (2.22) is hyperbolic if* $c_1 > 0$.

Usually the strict concavity of the entropy holds for $\tau_1 > 0, \varepsilon_1 > 0$, so that the domain of hyperbolicity of (2.22) is $\{c_1, \tau, u, e \in \mathbb{R}^4, c_1 > 0, \tau > 0, e - \frac{u^2}{2} > 0\}$.

Note that $s = \sqrt{-\omega}$ appears as the sound speed (in Lagrangian coordinates) in the medium consisting in the mixing of the compressible fluid and the unde-

formable solid,

$$s = \sqrt{-\omega} = \sqrt{-\frac{1}{c_1}\frac{\partial p_1}{\partial \tau_1}} = \sqrt{\frac{1}{c_1}\frac{s_1^2}{\tau_1^2}} = \frac{s_1}{\sqrt{c_1}\frac{\tau_1}{\tau}}$$

where s_1 is the sound speed (in Lagrangian coordinates) in the fluid, given by $s_1 = \sqrt{\gamma_1(p_1(\tau_1, \varepsilon_1) + \pi_1)\tau_1}$. Thus the sound speed of the mixing has a singularity when c_1 tends to 0. Let us end this subsection by giving the expression of the expression of the strictly concave classical entropy for a stiffened gas: $S_1(\tau_1, \varepsilon_1) = (p_1(\tau_1, \varepsilon_1) + \pi_1)\tau_1^{\gamma_1}$.

2.4. Numerical algorithm

Here we present the numerical scheme we developed to solve the one dimensional problem. It is based on the "Lagrange-projection" algorithm analyzed by Després: [7], [8]; this is an explicit finite volume method. The general procedure consists in an operator splitting whose first step solves (2.22) (Lagrange stage) and whose second step solves $\mathrm{D}_t V = 0$ (projection, or convection step) where V is the vector of all the transported unknowns.

In this subsection, we assume a mesh with cells of constant size Δx is given and, for every $j \in \mathbb{Z}$, $n \in \mathbb{N}$, denote by z_j^n the approximate value of the quantity z at $j\Delta x$ and at time $n\Delta t$ (in the naive assumption that Δt remains constant). Without recalling basic definitions of finite volume schemes, we here briefly discuss how to compute $(z_j^{n+1})_{j\in\mathbb{Z}}$ from $(z_j^n)_{j\in\mathbb{Z}}$, z representing any of the variables in (2.21). In the following, we skip the time index n (but not $n+1$).

The Lagrange step's role is to solve (2.22). The use of an explicit method and equation $\rho \mathrm{D}_t p_1 = \omega \partial_x u$ of the symmetrized system suggest that a CFL condition of order $\sqrt{-\omega}\Delta t/\Delta x \leq 1$ will have to be imposed in order the scheme to be stable. This is constraintfull because nothing plays against the rarefaction of the fluid in any cell: a dramatic decrease of the time step is predictable when the solid occupies almost a whole cell (ω is of order $1/c_1$). In order to avoid this problem, we propose a derefinement procedure (that will have to be followed by a refinement one). The general design of the algorithm is then the following:

- derefinement (z_j becomes $\overline{z_j}$),
- Lagrange step ($\overline{z_j}$ becomes $\widetilde{z_j}$),
- projection step ($\widetilde{z_j}$ becomes $\widehat{z_j}$),
- refinement ($\widehat{z_j}$ becomes z_j^{n+1}),
- computation of the new velocity of the solid (with Newton's laws).

2.4.1. Derefinement This part of the algorithm takes advantage of the fact that mixed cells are very localized: in dimension 1, each boundary of the solid intersects at most one cell. We thus know that any mixed cell is located near a pure fluid cell. The principle is here to consider the mixed cell with its pure fluid neighbor as a unique big cell. This allows to recover a volume fraction of fluid $c_1\tau_1/\tau > 1/2$ in the whole computational domain.

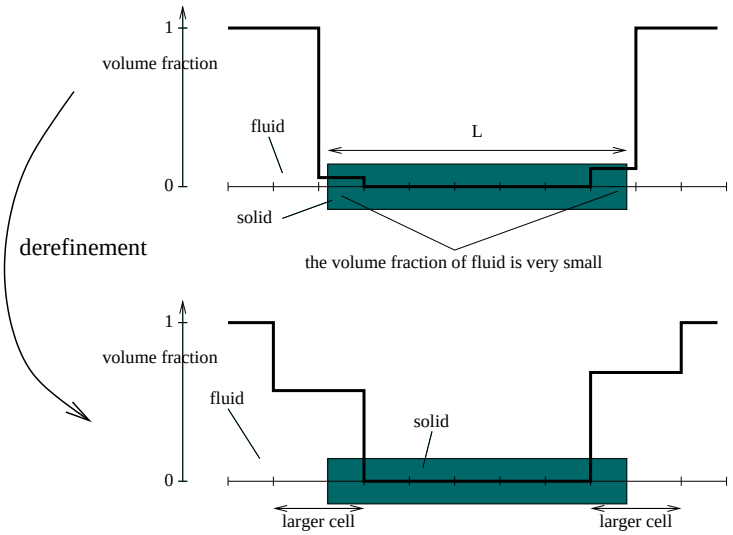

Figure 6: Derefinement

The derefinement algorithm is the following.

- Detect cells where $c_1\tau_1/\tau < 1/2$, let us say cell j.
- For each of these cells, detect the neighbor cell where $c_1 = 1$ (in the other neighbor, $c_1 = 0$): assume for example it is cell $j-1$.
- In the mixed cell j and its neighbor $j-1$, replace all conservative quantities ρ, ρc_1, ρu, ρe by their mean values on j and $j-1$:

$$\begin{cases} \overline{\rho_{j-1}} = \overline{\rho_j} = (\rho_{j-1} + \rho_j)/2, \\ \overline{\rho_{j-1}c_{1,j-1}} = \overline{\rho_j c_{1,j}} = (\rho_{j-1}c_{1,j-1} + \rho_j c_{1,j})/2, \\ \overline{\rho_{j-1}u_{j-1}} = \overline{\rho_j u_j} = (\rho_{j-1}u_{j-1} + \rho_j u_j)/2, \\ \overline{\rho_{j-1}e_{j-1}} = \overline{\rho_j e_j} = (\rho_{j-1}e_{j-1} + \rho_j e_j)/2, \end{cases}$$

  (and new values of τ_1, ε_1, p_1... follow).
- In the other cells, values are unchanged: $\overline{z_k} = z_k$;

The consequence of this trick is that $c_1\tau_1/\tau > 1/2$ in each cell, so that

$$s = \frac{s_1}{\sqrt{c_1}\frac{\tau_1}{\tau}} = \frac{\sqrt{c_1}s_1}{c_1\frac{\tau_1}{\tau}} \leq 2\sqrt{c_1}s_1 \leq 2s_1$$

if $c_1 \in]0,1]$. Thus the sound speed of the mixing (where $c_1 > 0$) is bounded if the one of the fluid is.

Remark 2.2. This derefinement produces an artificial spreading (diffusion) of the solid.

2.4.2. Lagrange step This part of the algorithm, so as the following, is directly taken from the Lagrange-projection schemes of [7] and [8] (and we here do not go further in explanations). The Lagrange stage solves (2.21). It relies on the definition of the cell edge quantities

$$\begin{cases} \rho s^*_{j+1/2} = \sqrt{\max(\rho_j {s_j}^2, \rho_{j+1} {s_{j+1}}^2)\min(\rho_j, \rho_{j+1})}, \\ p_{j+1/2} = \dfrac{p_j + p_{j+1}}{2} + \dfrac{\rho s^*_{j+1/2}}{2}(u_j - u_{j+1}), \\ u_{j+1/2} = \dfrac{p_j - p_{j+1}}{2\rho s^*_{j+1/2}} + \dfrac{1}{2}(u_j + u_{j+1}), \end{cases}$$

with $p_j = p_1(\tau_{1,j}, \varepsilon_{1,j})$ and $s_j = s_1(\tau_{1,j}, \varepsilon_{1,j})\tau_j/(\sqrt{c_{1,j}}\tau_{1,j})$ (s is the sound speed in the global fluid in Lagrangian coordinates).

Remark 2.3. The Lagrangian edge quantities are evaluated on the discrete solution *before* the derefinement.

These edge quantities allow to compute all the variables after the Lagrange step with formulae

$$\begin{cases} \widetilde{c_{1,j}} - \overline{c_{1,j}} = 0, \\ \overline{\rho_j}\dfrac{\widetilde{\tau_j} - \overline{\tau_j}}{\Delta t} - \dfrac{u_{j+1/2} - u_{j-1/2}}{\Delta x} = 0, \\ \overline{\rho_j}\dfrac{\widetilde{u_j} - \overline{u_j}}{\Delta t} + \dfrac{p_{j+1/2} - p_{j-1/2}}{\Delta x} = 0, \\ \overline{\rho_j}\dfrac{\widetilde{e_j} - \overline{e_j}}{\Delta t} + \dfrac{p_{j+1/2}u_{j+1/2} - p_{j-1/2}u_{j-1/2}}{\Delta x} = 0, \end{cases} \tag{2.23}$$

with $\overline{\tau_j} = 1/\overline{\rho_j}$ for every cell (for all j).

The contact between fluid and solid are treated as wall conditions with imposed velocity of the wall (pragmatically, this is a way to obtain edge values $p_{j+1/2}$, $u_{j+1/2}$ at the contact with pure solid that lead to a stable scheme).

2.4.3. Projection step This step of the algorithm can be viewed as a remapping part. It solves the advection system

$$\begin{cases} \partial_t c_1 + u\partial_x c_1 = 0, \\ \partial_t \rho + u\partial_x \rho = 0, \\ \partial_t u + u\partial_x u = 0, \\ \partial_t e + u\partial_x e = 0. \end{cases} \tag{2.24}$$

In the chosen discrete version, the fluxes $\widetilde{z_{j+1/2}}$ are computed following the following procedure (as in [16]):

- First, compute the mass fraction fluxes *exactly*, which is easy because the velocity inside the solid is constant in space and in time during the whole time step: denote it $\widetilde{c_{1,j+1/2}}$ and $\widetilde{c_{2,j+1/2}}$, of course verifying $\widetilde{c_{1,j+1/2}}+\widetilde{c_{2,j+1/2}}=1$.

- Second, compute the upwinded fluxes for the fluid specific volume, the fluid internal energy, the solid specific volume and the velocity:

$$\left\{\begin{array}{l}
\widetilde{\tau_{1,j+1/2}}=\widetilde{\tau_{1,j}} \text{ if } u_{j+1/2}\geq 0,\\
\widetilde{\tau_{1,j+1/2}}=\widetilde{\tau_{1,j+1}} \text{ if } u_{j+1/2}<0,\\
\widetilde{\varepsilon_{1,j+1/2}}=\widetilde{\varepsilon_{1,j}} \text{ if } u_{j+1/2}\geq 0,\\
\widetilde{\varepsilon_{1,j+1/2}}=\widetilde{\varepsilon_{1,j+1}} \text{ if } u_{j+1/2}<0,\\
\widetilde{\tau_{2,j+1/2}}=\tau_2,\\
\widetilde{u_{j+1/2}}=\widetilde{u_j} \text{ if } u_{j+1/2}\geq 0,\\
\widetilde{u_{j+1/2}}=\widetilde{u_{j+1}} \text{ if } u_{j+1/2}<0.
\end{array}\right.$$

- Third, compute the conservative fluxes with

$$\left\{\begin{array}{l}
\widetilde{\rho_{j+1/2}}=\dfrac{1}{\widetilde{c_{1,j}}\widetilde{\tau_{1,j+1/2}}+\widetilde{c_{2,j}}\widetilde{\tau_{2,j+1/2}}},\\
\widetilde{e_{j+1/2}}=\widetilde{c_{1,j}}\widetilde{\varepsilon_{1,j+1/2}}+\dfrac{\widetilde{u_{j+1/2}}^2}{2}.
\end{array}\right.$$

$$\left\{\begin{array}{l}
\dfrac{\widehat{\rho_j}\widehat{c_{1,j}}-\widetilde{\rho_j}\widetilde{c_{1,j}}}{\Delta t}+u_{j-1/2}\dfrac{\widetilde{\rho_{j+1/2}}\widetilde{c_{1,j+1/2}}-\widetilde{\rho_{j-1/2}}\widetilde{c_{1,j-1/2}}}{\Delta x}=0,\\
\dfrac{\widehat{\rho_j}-\widetilde{\rho_j}}{\Delta t}+u_{j-1/2}\dfrac{\widetilde{\rho_{j+1/2}}-\widetilde{\rho_{j-1/2}}}{\Delta x}=0,\\
\dfrac{\widehat{\rho_j}\widehat{u_j}-\widetilde{\rho_j}\widetilde{u_j}}{\Delta t}+u_{j-1/2}\dfrac{\widetilde{\rho_{j+1/2}}\widetilde{u_{j+1/2}}-\widetilde{\rho_{j-1/2}}\widetilde{u_{j-1/2}}}{\Delta x}=0,\\
\dfrac{\widehat{\rho_j}\widehat{e_j}-\widetilde{\rho_j}\widetilde{e_j}}{\Delta t}+u_{j-1/2}\dfrac{\widetilde{\rho_{j+1/2}}\widetilde{e_{j+1/2}}-\widetilde{\rho_{j-1/2}}\widetilde{e_{j-1/2}}}{\Delta x}=0
\end{array}\right.$$

2.4.4. Refinement The aim of this part is to recover a constant-by-cell approximation (on the original little cells of the mesh) and to balance the artificial spreading of the derefinement phase (cf. remark 2.2). It only concerns the cells where $\widehat{c_{1,j}}(1-\widehat{c_{1,j}})>0$. Without entering the details (that are tedious), let us just mention that this last step of the time iterate globally conserves

- volume fraction of fluid and solid,
- mass fraction of fluid and solid,
- total momentum,
- total energy

on the two neighbor cells that are concerned.

2.4.5. New evaluation of the velocity of the solid The new velocity v^{n+1} of the solid is simply computed using Newton's laws. Let us denote by L the length of the solid and j_l, j_r the indices of the mixed cells respectively on the left and on the right of the solid. The discrete velocity evolution is

$$v^{n+1} = v - \frac{\Delta t}{L}\tau_2(p_{j_r-1/2} - p_{j_l+1/2}).$$

Remark 2.4. The present scheme is by construction conservative in mass and momentum. Nevertheless, it is not conservative in total energy: this is due to the fact that the new evaluation of the solid velocity is done via the momentum fluxes on the mixed cell edges, and the new solid energy, $1/2{v^{n+1}}^2$, does not coincide with the ancient one updated via the energy fluxes on the mixed cell edges. This phenomenon can be compared with the so-called "wall heating" that occurs in pure fluid cells, but there, the difference is reported in the internal energy (which is not taken into account in the solid). The lack of energy conservation is a general drawback of coupled fluid-solid numerical systems, even in moving meshes formulation, as reported and studied in [25].
The evolution of total energy in time is reported in graph 13 in subsection 2.5.

2.5. Some numerical results

Let us now present some numerical results for the following simulation: in the interval $[0, 1]$ limited with wall condition on both sides, a solid of density 20 and length 0.1 (thus with mass 2) is initially centered on 0.5 and has velocity 100. The fluid on both sides is an ideal gas with $\gamma_1 = 2$, $\pi_1 = 0$ and is initially at rest with pressure equal to 1 and density equal to 1.

This model problem is very similar to the one studied in [24].

We present three numerical results obtained for $t = 0.001$, $t = 0.0051$ (the solid being at its extremal position on the right) and $t = 0.016$ (the solid being at its extremal position on the left), with three different meshes : 100, 300 and 1000 cells. We note a relatively slow convergence for the velocity, particularly at time $t = 0.016$. What is remarkable is that although the velocity of the solid seems far to be converged, the position of the solid is good. The reason is that the acceleration of the solid at its extremal position is important, so that a small error in time gives a huge error for the velocity.

Figure 13 shows the evolution of total energy in the whole domain. It seems to converge to a conserved quantity when refining the mesh, as expected. The variation of the total energy seems to be an increasing function of the accelaration of the solid, but a more precise study should be done to allow a precise analysis of the phenomenon.

We at last present a result obtained in the same general conditions but with $\pi_0 = 100000$. Figure 14 (with 200 cells) shows the pressure at time $t = 0.0024$: the solid is at his extremal position on the left. Of course, this position is more on the left than on the preceding figures for time $t = 0.0051$, this is due to the fact

that the fluid is now stiffer. The pressure inside the solid is by convention fixed to 1, but this does not affect the computation.

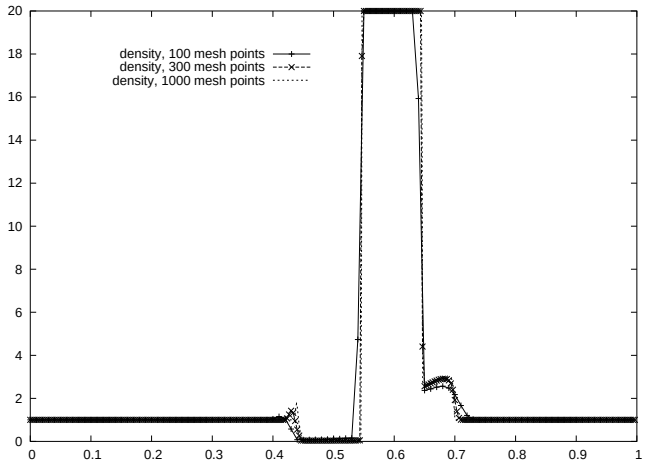

Figure 7: Density, time $t = 0.001$.

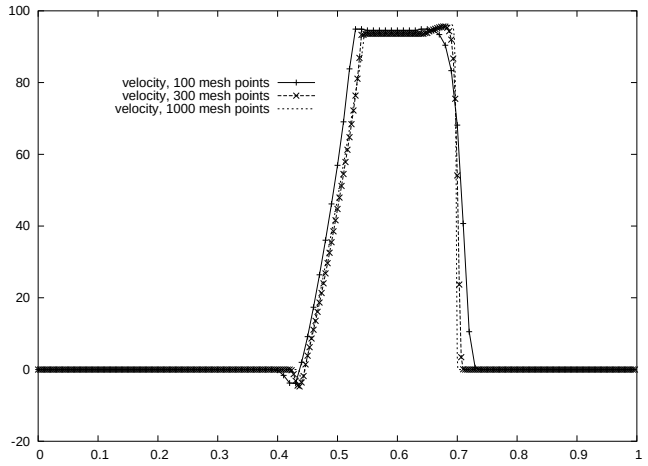

Figure 8: Velocity, time $t = 0.001$.

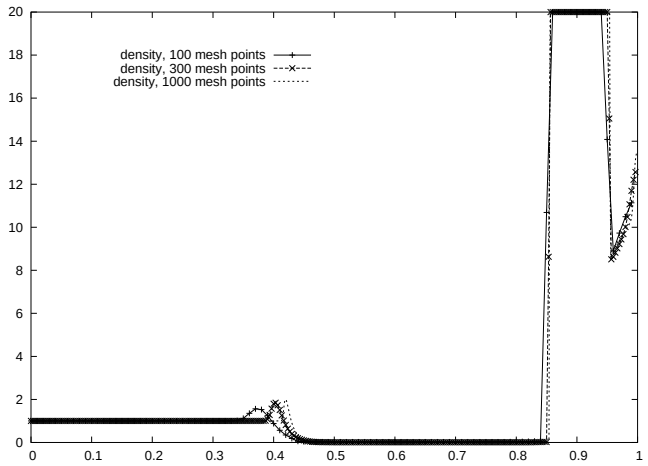

Figure 9: Density, time $t = 0.0051$.

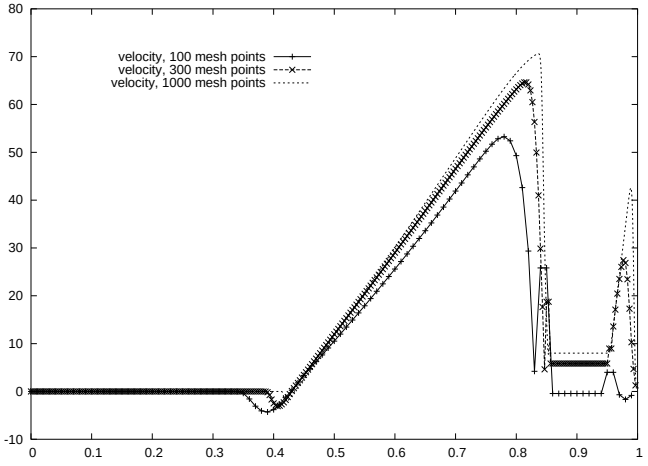

Figure 10: Velocity, time $t = 0.0051$.

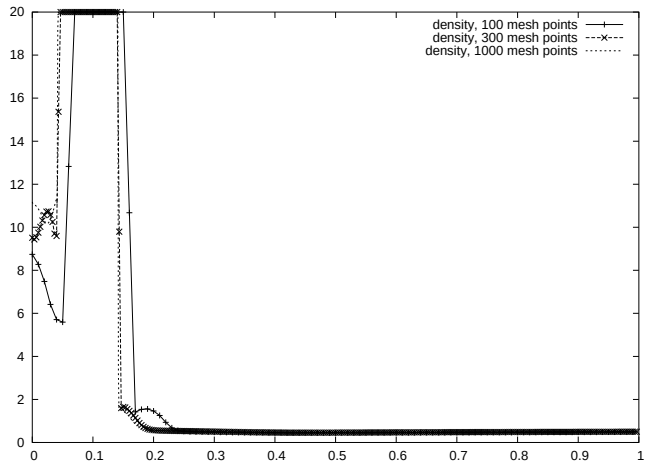

Figure 11: Density, time $t = 0.016$.

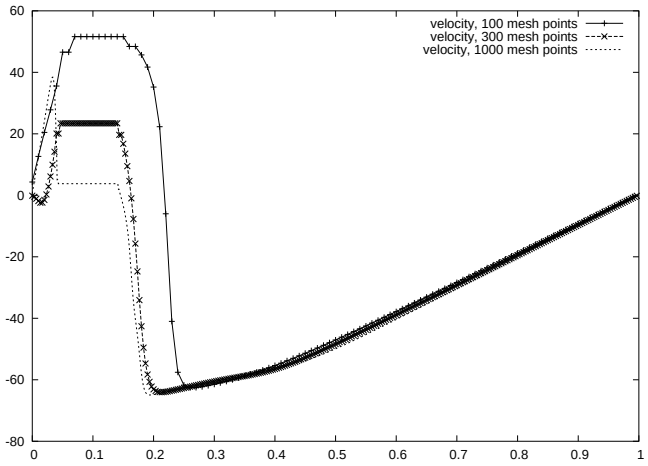

Figure 12: Velocity, time $t = 0.016$.

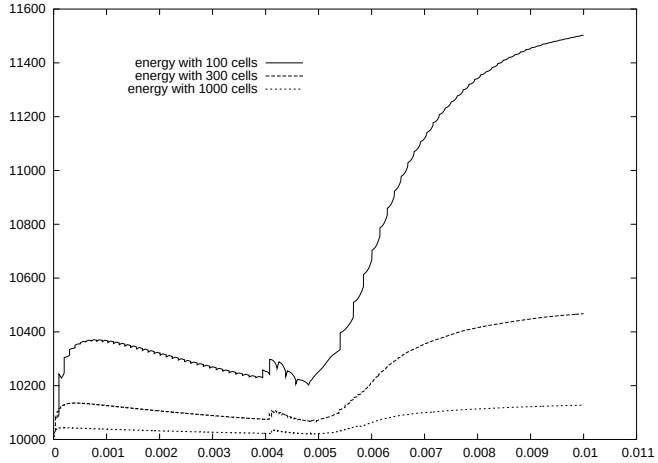

Figure 13: Total energy in $[0, 1]$ as a function of time.

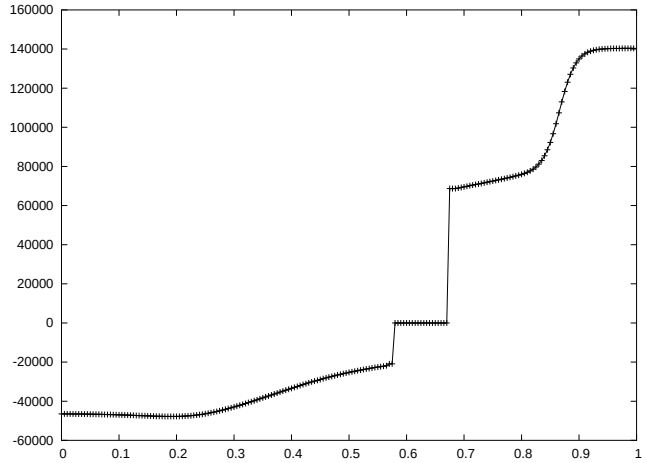

Figure 14: Pressure with $\pi_1 = 100000$, 200 cells, time $t = 0.0024$.

A conclusion of this part could be as follows. We developed an algorithm to solve the coupled compressible Euler system with the motion of a rigid body. One important feature of the algorithm is that it only need a unique Cartesian mesh. For the sake of simplicity, we chose an explicit solving of the problem, which is known to require a CFL-like condition that prescribes an upper bound for the time steps Δt. This upper bound is a function of the length of the fluid cell. In order not to dramatically reduce the time step due to the existence of cells that are almost empty of fluid, we developed a derefinement, or projection, procedure. The

rest of the algorithm uses a classical Lagrange-Projection solver (for which some stability results, via entropy inequalities, are available). Some comparison with results obtained by ALE methods on moving meshes will be done in an immediate future to evaluate the error due to this projection on larger cells in the area of the interface between the fluid and the solid. Finally, dimensional splitting to two and three dimensional computations have to be done to demonstrate the interest of this method.

References

[1] A. A. Amsden, Kiva-3V, release 2, improvements to Kiva-3V. Report # LA-UR-99-915, Los Alamos National Laboratory, 1999.

[2] C. Baranger, Modeling of oscillations, breakup and collisions for droplets: the establishment of kernels for the T.A.B. model. To appear in *Math. Models Methods Appl. Sci.*

[3] C. Baranger and L. Desvilettes, Study at the numerical level of the kernels of collision, coalescence and fragmentation for sprays. To appear in *Proceedings of the International Workshop on Multiphase and Complex Flow Simulation for Industry, Cargèse, France, 2003*

[4] S. D. Bauman, A spray model for an adaptive mesh refinement code. PhD Thesis, University of Wisconsin - Madison, 2001.

[5] L. Boudin, L. Desvillettes and R. Motte, A modeling of compressible droplets in a fluid. *Comm. Math. Sci.*, **1** (2003), 657–669.

[6] B. Desjardins and M. Esteban, On weak solutions for fluid-rigid structure interaction: compressible and incompressible models, *Comm. Partial Differential Equations*, **25** (2000), 1399–1413.

[7] B. Després, Lagrangian systems of conservation laws. Invariance properties of Lagrangian systems of conservation laws, approximate Riemann solvers and the entropy condition. *Numer. Math.*, **89** (2001), no. 1, 99–134.

[8] B. Després, Symétrisation en variable de Lagrange pour la mécanique des milieux continus et schémas numériques, *MATAPLI*, **72** (2003), 45–61.

[9] C. Farhat, B. Larrouturou and S. Piperno, Partitioned procedures for the transient solution of coupled aeroelastic problems I: model problem, theory and two-dimensional application, *Comput. Methods Appl. Mech. Engrg.*, **124** (1995), no. 1-2, 79–112.

[10] E. Feireisl, On the motion of rigid bodies in a viscous compressible fluid, *Arch. Ration. Mech. Anal.*, **167** (4):281–308, 2003.

[11] R. Glowinski, T.-W. Pan, T. I. Hesla, D. D. Joseph, and J. Périaux, A fictitious domain approach to the direct numerical simulation of incompressible viscous flow past moving rigid bodies: application to particulate flow, *J. Comput. Phys.*, **169** (2):363–426, 2001.

[12] C. Grandmont and Y. Maday, Existence for an unsteady fluid-structure interaction problem, *M2AN Math. Model. Numer. Anal.*, **34** (2000), 609–636.

[13] M. Gunzburger, H.-C. Lee and G. Seregin, Global existence of weak solutions for viscous incompressible flows around a moving rigid body in three dimensions, *J. Math. Fluid Mech.*, **2** (2000), 219–266.

[14] J.J. Hylkema, Modélisation cinétique et simulation numérique d'un brouillard dense de gouttelettes. Application aux propulseurs à poudre. PhD Thesis, Université Toulouse-III, 1999.

[15] M. Ismail, Simulation d'Écoulements fluide-particules par la FBM. PhD Thesis, Université Paris-VI (2004).

[16] F. Lagoutière, Modélisation mathématique et résolution numérique de problèmes de fluides à plusieurs constituants. PhD thesis, Université Paris-VI (2000).

[17] B. Maury, Direct Simulations of 2D Fluid-Particle Flows in Biperiodic Domains. *J. Comput. Phys.*, **156** (1999), 325–351.

[18] B. Maury, A Fat Boundary Method for the Poisson problem in a domain with holes. *J. Sci. Comput.*, **16** (3) (2001), 319–339.

[19] P. Métier, Modélisation, analyse mathématique et applications numériques de problèmes d'interaction fluide-structure instationnaires. PhD Thesis, Université Paris-VI (2003).

[20] P. J. O'Rourke, Collective drop effects on vaporizing liquid sprays. PhD Thesis, Los Alamos National Laboratory, 1981.

[21] M. A. Patterson and R. D. Reitz, Modeling the effects of fuel spray characteristics on Diesel engine combustion and emissions. *SAE paper* #980131, 1998.

[22] C. S. Peskin, Flow patterns around heart valves: a digital computer method for solving the equations of motion. PhD Thesis, Albert Einstein College of Medicine, 1972.

[23] C. S. Peskin, The immersed boundary method. *Acta Numer.*, **11** (2002), 479–517.

[24] S. Piperno, Explicit/implicit fluid/structure staggered procedures with a structural predictor and fluid sub-cycling for 2D inviscid aeroelastic simulations, *Internat. J. Numer. Methods Fluids*, **25** (1997), no. 10, 1207–1226.

[25] S. Piperno, Contribution à l'étude mathématique et à la simulation numérique de phénomènes d'interaction fluide-structure, habilitation à diriger des recherches, Université Paris-VI, 2000.

[26] W. E. Ranz and W. R. Marshall, Vaporization from drops, part I-II. *Chem. Eng. Prog.*, **48** (3) (1952), 141–180.

[27] R. D. Reitz, Modeling atomization processes in high-pressure vaporizing sprays. *Atom. Spray Tech.*, **3** (1987), 309–337.

[28] J. San Martín, J. F. Scheid, T. Takahashi and M. Tucsnak, Convergence of the Lagrange-Galerkin method for the Equations Modelling the Motion of a Fluid-Rigid System, preprint.

[29] J. San Martín, V. Starovoitov, and M. Tucsnak, Global weak solutions for the two-dimensional motion of several rigid bodies in an incompressible viscous fluid, *Arch. Ration. Mech. Anal.*, **161** (2002), 113–147.

[30] T. Takahashi, Analyse des équations modélisant le mouvement des systèmes couplant des solides rigides et des fluides visqueux, PhD Thesis, Université Nancy-I, 2002.

[31] S. Vincent, J.-P. Caltagirone, M. Azaiez and N. Randrianarivelo, Méthodes de pénalisation pour les équations de Navier-Stokes. Application à l'interaction fluide/structure, oral communication at J.-L. Lions laboratory, January 20th, 2003.

[32] F. A. Williams, *Combustion theory*, second edition, Benjamin Cummings, 1985.